V European Conference on Computational Fluid Dynamics
ECCOMAS CFD 2010
J. C. F. Pereira and A. Sequeira (Eds)
Lisbon, Portugal, 14–17 June 2010

INVERSE AND DIRECT TECHNIQUES OF THE HEAT TRANSFER COEFFICIENT RETRIEVAL IN IMPINGEMENT JET HEAT EXCHANGE

Ryszard Białecki[*] and Arkadiusz Ryfa[†]

[*]Institute of Thermal Technology, Silesian University of Technology
Konarskiego 22, 44-100 Gliwice, Poland
e-mail: Ryszard.Bialecki@polsl.pl

[†]Institute of Thermal Technology, Silesian University of Technology
Konarskiego 22, 44-100 Gliwice, Poland
Arkadiusz.Ryfa@polsl.pl

Key words: Inverse methods, heat transfer coefficient, CFD, impingement jet.

Abstract. *The paper presents an inverse technique for obtaining spatial distribution of the heat transfer coefficient (HTC) for the impingement jet heat exchange problem. Two models of the temperature field in the solid impinged by the jet are derived. The first results from the parameterization of the unknown temperature at the impingement surface, the second from the parameterization of the unknown heat flux at the same surface. Resorting to the assumed linearity of the heat conduction problem, both models express the temperature field as a linear combination of auxiliary fields. Each of these fields is evaluated by solving a simple forward problem. Simultaneous minimization of the discrepancies between measured temperatures and both models with an additional constraint enforcing the temporal invariability of the HTC, produces the spatial distribution of the latter. Measurements by infrared camera were used to retrieve HTC for different geometrical configurations. Reasonable agreement of the inverse analysis with CFD simulations of an conjugate convection-conduction problem was found. The CFD model was also used to verify the assumed temporal invariability of HTC.*

1 INTRODUCTION

Jet impingement is a method of intensifying heat exchange. It involves a jet flow from a nozzle to a targeted surface [1]. The destruction of the boundary layer by the momentum of the fluid leads to high, local and surface averaged, heat transfer coefficients. Cooling of crucial parts of car and aircraft engines, turbine blades, electronics, paper and textile drying, ingot cooling in metallurgy, removal and/or prevention of ice on aircraft components and aluminum annealing, are just few examples where impingement cooling is employed. Practical application of this technique of enhancement of heat transfer requires a development of tools for predicting the intensity of the energy transfer at the impinged surfaces.

Coupled analysis is one of techniques of simulating the heat flow in the solid and the surrounding fluid. In this approach the mass, momentum and energy transfer problems in the fluid and the heat conduction problem in the solid are solved simultaneously. Temperature fields in the fluid and solid are coupled by enforcing continuity of temperature and heat flux on the interface. In many cases conjugate analysis, though conceptually straightforward, is not the optimal technique of solving the heat transfer problem. An alternative approach is to solve the problem in the fluid and the solid separately. The reason for selecting such a technique is often prohibitively long computing times or insufficient accuracy of the computational fluid dynamics (CFD). To use such a segregated technique, the boundary conditions (BC) on the surface bounding the solid, need to be defined. The most frequently used types of BC's are the Dirichlet data (prescribed temperature), the Neumann (prescribed heat flux) and Robin (prescribed heat transfer coefficient and temperature of the fluid exchanging heat with the solid). The necessary data on the boundary can be obtained by direct measurements (temperature), CFD analysis or inverse techniques. The later relies on a best fit of the modeled and measured temperature field in the solid, and as such requires additional measurements. As opposed to the direct measurements, the temperature sensors used in the inverse analysis need not necessarily be located on the solid-fluid interface. The CFD and inverse analysis can be used to retrieve any type of BC's. However, from the practical point of view, the distribution of the heat transfer coefficient (HTC) is the optimal BC to be retrieved. The reason for this is, that the HTC weakly depends on temperature, and in transient cases, also on time.

The CFD simulation of the single-phase submerged jet impingement problem has been widely addressed in literature. The behavior of various turbulence models in the context of gas turbine cooling was investigated in [2]. The problem of a concave surface cooling is addressed in [3] by Souris who also compared the k-ε and the Reynolds stress turbulence models (RSM) for several jet configurations. Similar problem is addressed in [4] where the simulation of micro jets for cooling of the electronic components is discussed. Large number of turbulence models has been validated against experimental data by Hofmann in [5].

Applying inverse analysis to retrieve the BC's on the impinged surface was discussed widely in the literature. Inverse problems for impingement thawing of frozen food have been discussed in [6]. It was found that the retrieved values of the HTC increases with the time of thawing. Reference [7] uses inverse technique to retrieve the values of local and stagnation point HTC at a water impinged surface while [8] addresses the determination of the heat flux. An application of the non iterative inverse algorithm for heat flux retrieval is given by Ling in [9]. The application of the inverse algorithm for HTC reconstruction for cooling of model of piston is addressed in [10].

The present paper differs from the earlier published techniques by resorting to the superposition principle to build the heat conduction model, simultaneous minimization of discrepancies resulting from retrieving the boundary flux and temperature as well as enforcing the constancy in time of the HTC coefficient. The contribution uses CFD both to validate some assumptions made when formulating the inverse problem and uses the CFD to validate

the results of the inverse analysis. The current study investigates a spatial distribution of the heat transfer coefficient for a single phase air jet. It presents the retrieval of the HTC, by forward and inverse procedures, for several different nozzle diameters in order to verify the so-called effective heat exchange area for each situation. Fluent, a commercial CFD code, is employed to simulate the fluid flow and the energy transfer in the air providing pipe, nozzle and in the vicinity of the heated object. The inverse algorithm is implemented in the authors' in-house code with the least square fitting of the mathematical model and measurements performed using a modified Levenberg-Marquardt method. This technique provides additional regularization allowing for reduction of the influence of the ill-posedness of the inverse problem on the results. The sensitivity coefficients required for the evaluation of the model temperatures were computed using MSC.Marc, a commercial FEM code.

2 EXPERIMENT

The single phase jet impingement experiment was carried out on the test rig schematically presented in Figure 1. The experiment involves an air jet heating a disk. The compressed ambient air is heated up by an electrical heater to 340K. The volumetric flow of air is measured by KME251 magnetic rotameter. All temperatures of the air are measured by k-type thermocouples. After the constant air parameters are reached, the valve is turned and the air starts flowing through the nozzle towards the sample. The heated object is a steel disc of 60mm diameter and 5mm thickness. The hot air impinges the front surface and the sample starts heating up. The temperature measurements are taken using a SC-2000 infrared camera on the back surface of the sample. The images are picked up every 0.2 seconds. The experiment was conducted for several nozzle diameters d as well as two nozzle-to-sample distances u being the two most important factors influencing the heat exchange process. The influence of the nozzle diameter on the jet heating efficiency was tested by using nozzles of diameters d equal to 5, 6 and 7mm.

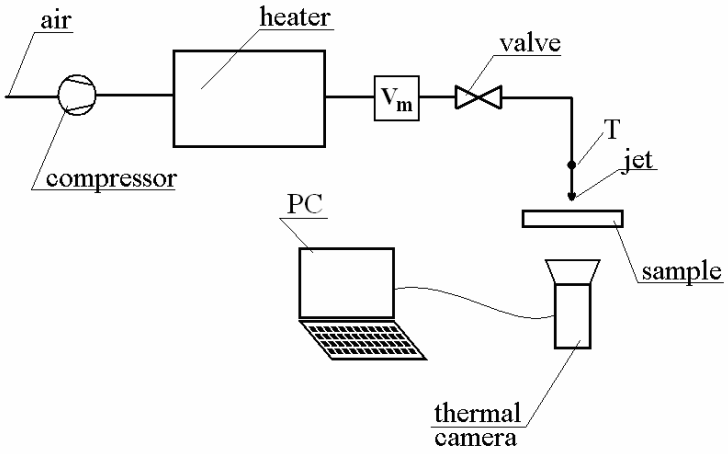

Figure 1: Sketch of the experimental rig.

Each nozzle was placed at the distance equal to 5 and 10 nozzle diameters from the sample. For each nozzle-sample configuration, the measurements last until the temperature field at the back of the sample reaches steady state. Each infrared camera picture encloses nearly 8000 temperature sensors (pixels) in the sample area. As the solution is axisymmetric the radius is divided on 38 equal segments. The temperature values for all pixels that belongs to the given segment are summed up. Then the average value is calculated. Therefore, every recorded frame is represented by 38 temperature values. The sampling time for an inverse analysis is taken as 1s. The measurement data from the thermal camera and the thermocouples in the pipe are stored on-line in the PC. Although the measurements show that the initial field

at the outer surface is not uniform it has been assumed constant. This is a simplification, but as the temperature field inside sample is unknown nothing more accurate could be considered. The initial temperature variation at the measured surface observed during measurements is between 0.1 and 0.3K.

3 CONJUGATE ANALYSIS

The geometry taken into consideration reproduced the real geometry of the experimental rig and encompassed a part of the pipe (0.5m) with the nozzle, the impinged disc and the surrounding air modelled as a cylinder of diameter 0.14m. The problem is formulated as axisymmetric.

Mass flow inlet was assumed at the inlet of the pipe. Outflow pressure conditions were prescribed on the fictitious boundary, where the air was leaving the computational domain. The correctness of these assumptions have been validated by appropriate sensitivity analysis. The domain was divided into 110k quad type elements with proper boundary layer. In regions of higher velocity and temperature gradients, i.e. the vicinity of the stagnation point and exit of the nozzle finer mesh has been generated. The final mesh density resulted from a mesh sensitivity study.

The time step varied during the analysis. In the initial period the time step was set to the 1e-4s, when the air impinged the heated object the time step had to be reduced to 1e-5s. After the flow started to slid along the surface, the time step was gradually increased. As soon as the flow field stabilized, a constant value equal to 0.001s was prescribed. During the initial simulation stage 35 internal iteration within a time step were required. Later on, the number of iterations was reduced to 5 per time step.

All simulations were performed with the SST k-ω turbulence model. This model has been recommended by Hoffman [5]. It has been reported as the only one that is able to reproduce the transition between stagnation and turbulent regions in the vicinity of the impingement point. To verify the assumption five turbulence models were tested. The spatial distribution of the HTC is presented in Figure 2.

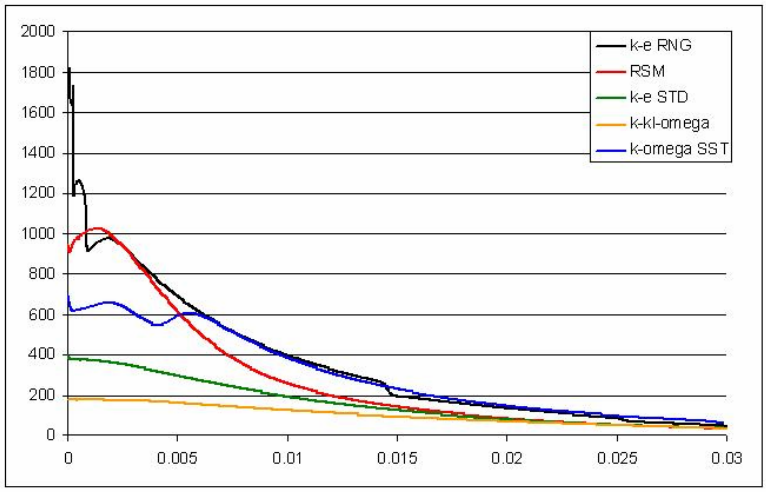

Figure 2: Spatial distribution of the HTC for various turbulence models.

The main conclusion is that no turbulence model can reproduce the HTC correctly. The k-ε RNG and RSM highly overpredict, while the k-kl-ω strongly underpredicts the HTC in the stagnation zone. The standard k-ε and k-ω SST give most probable values. Out of those two only the latter one shows proper behaviour of the HTC in the transition zone [5]. Yet still the values given by this model are overshot [5]. The measurements carried out within this work

confirm also this behaviour. As the k-ω model gave the best results it was used for all further simulations.

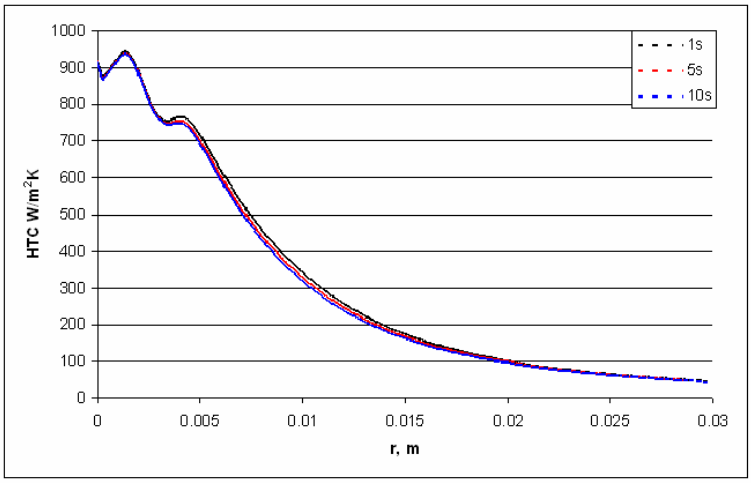

Figure 3: Spatial distribution of the HTC for various time instances.

The main assumption of the developed inverse algorithm is the invariance of the HTC in time. This assumption has been validated by conjugate CFD simulations. Results presented in Figure 3, shows that the HTC exhibits no variation over time, so the correctness of the assumption is confirmed.

4 INVERSE TECHNIQUE

The inverse algorithm presented in this paper is an extension of our earlier work [10]. Previously, the HTC was calculated using the *time to arrival* technique using thermochromic paints. The HTC was evaluated indirectly from retrieved boundary temperature and a heat flux. The method presented in this paper retrieves the HTC directly from the transient temperature measurements carried out using infrared camera and performed at the surface opposite to the impinged one. The unknown boundary distributions of heat flux and temperature are parameterized by expressing them as a linear combination of simple functions of compact support. Resorting to the linear dependence of the temperature field on the boundary heat flux and temperature, the temperature distribution in the domain, can be expressed as a linear combination of some readily computed auxiliary fields. Least squares fit of the model and the measurements yields then the values of the coefficients of this combination.

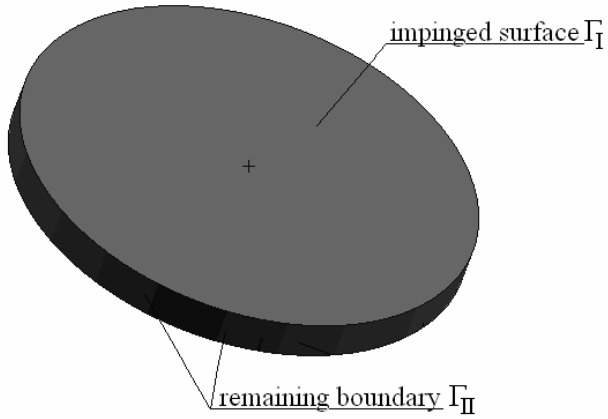

Figure 4. The impinged sample and boundary division.

Figure 4 shows a configuration of the domain under consideration. The domain Ω bounded by a surface Γ is divided into two parts. On the first part Γ_I the heat flux q_I is unknown. On the remaining portion of the boundary, denoted by Γ_{II}, the boundary conditions are known.

It is assumed that the problem is linear, so that the temperature field in the domain can be expressed as the sum of two temperature fields:

$$T(\mathbf{r},\tau) = T_I(\mathbf{r},\tau) + T_{II}(\mathbf{r},\tau) \tag{1}$$

where the T_{II} is the temperature field corresponding to the zero flux prescribed on Γ_I, initial condition, boundary conditions on Γ_{II} and the internal heat generation as in the original problem. Such a problem is a well defined forward one and as such can be solved with any standard technique. The second temperature field T_I corresponds to homogeneous initial and boundary conditions on Γ_{II}, the actual heat flux on the boundary Γ_I and no internal heat generation. Temperature field T_I is unknown as it depends on the distribution of the heat flux on Γ_I. To evaluate this field the searched heat flux is expressed as a linear combination of known compact support space dependent trial functions N_k, and time dependent linear shape functions M_n (Figure 5).

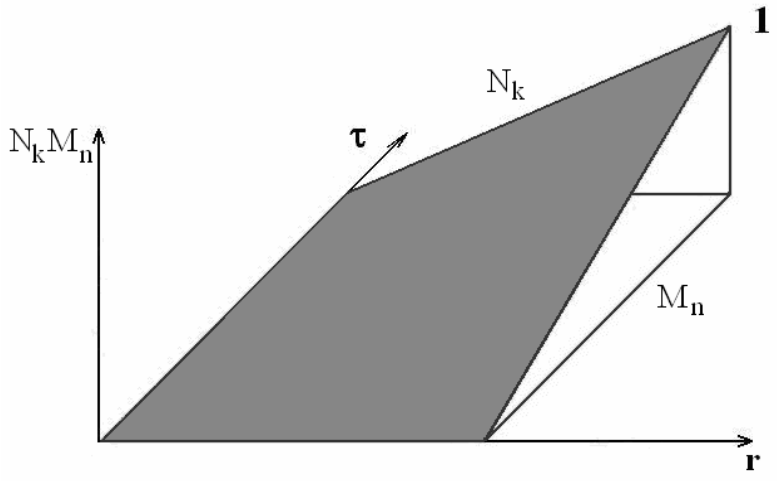

Figure 5. The time and space trial functions.

The searched heat flux is expressed as the linear combination of the mentioned above trial functions N_k and unknown scalars q_k^b and q_k^e

$$q_I(\mathbf{r},\tau) = \sum_{k=1}^{K} q_k^b N_k(\mathbf{r}) M_n^b(\tau) + \sum_{k=1}^{K} q_k^e N_k(\mathbf{r}) M_n^b(\tau) \tag{2}$$

In this work, the trial functions are selected to have the finite element shape function properties. It means that each trial function is associated with its nodal point, where the function assumes the value of 1. At all remaining nodes the function vanishes. With such an interpretation, the unknown scalars q_k^b and q_k^e can be interpreted as the values of the heat fluxes at appropriate nodal points. Indices *b* and *e* correspond to the begin and end of the selected time interval where the approximation is valid.

In the present study, the sample is a flat cylindrical plate, The front surface Γ_I, is a surface where the HTC is retrieved while the remaining part of the boundary Γ_{II} is insulated. The HTC is described by a set of three approximation (trial) functions. First is a cone with its axis at the stagnation point. The height of the function at the stagnation point is equal to one and

decays linearly with the distance from this point until r = 0.009m. The second function equals to 0 at the stagnation point and grows with the increasing radius. It reaches 1 at r = 0.009m, decaying to 0 at r = 0.018m. For r>0.018m spatially constant trial function are used, as the variation of the heat flux is small in this region,

Approximation (2) and the linearity of the problem leads to a simple formula that links the temperature at Γ_I, further denoted as T_I , with the unknown coefficients q_k^b and q_k^e

$$T_I(\mathbf{r},\tau) = \sum_{k=1}^{K} q_k^b \Theta_k^b(\mathbf{r},\tau) + \sum_{k=1}^{K} q_k^e \Theta_k^e(\mathbf{r},\tau) \tag{3}$$

Where Θ_k^b and Θ_k^e are temperature fields obtained after prescribing on Γ_I heat fluxes $N_k(\mathbf{r})M_n^e(\tau)$ and $N_k(\mathbf{r})M_n^e(\tau)$, respectively. The remaining boundary conditions, the initial condition and the governing equation are in this case homogeneous. With these assumptions, the auxiliary temperature fields Θ_k^b and Θ_k^e can be determined by solving a forward problem using any standard analytical or numerical technique. In this paper all forward problems are solved using a commercial FEM code MSC.Marc.

Inserting expression (3) into (1) produces

$$T(\mathbf{r},\tau) = \sum_{k=1}^{K} q_k^b \Theta_k^b(\mathbf{r},\tau) + \sum_{k=1}^{K} q_k^e \Theta_k^e(\mathbf{r},\tau) + T_{II}(\mathbf{r},\tau) \tag{4}$$

Defining the sensitivity coefficient as the derivative of the temperature field with respect to the unknown parameter, shows that the auxiliary fields Θ can be interpreted as distributions of the sensitivity coefficients.

$$j_k^p = \frac{\partial T(\mathbf{r},\tau)}{\partial q_k^p} = \Theta_k^p(\mathbf{r},\tau) \tag{5}$$

where the index p equals to either e or b. Sampling the temperature field (4) at sensor locations $\mathbf{r}_i$, i=1,2,…I and time instant τ_l, l=1,2,…L produces an overdetermined set of linear equations that can be cast in a matrix form as

$$\mathbf{T} = \mathbf{J}_q^b \mathbf{q}^b + \mathbf{J}_q^e \mathbf{q}^e + \mathbf{T}_{II} \tag{6}$$

where the vectors $\mathbf{q}^b$ and $\mathbf{q}^e$ are sets of sought for fluxes at the begin and end of the time step, respectively. $\mathbf{T}$ and $\mathbf{T}_{II}$ are vectors collecting temperatures $T(\mathbf{r}_i, \tau_l)$ and $T_{II}(\mathbf{r}_i, \tau_l)$ sampled at measurement points and times. $\mathbf{J}_q^b$ and $\mathbf{J}_q^e$ are Jacobi matrices whose entries are defined as $\{\mathbf{J}_q^b\}_{sk} = \Theta_k^b(\mathbf{r}_i,\tau_l)$; $\{\mathbf{J}_q^e\}_{sk} = \Theta_k^e(\mathbf{r}_i,\tau_l)$; Subscript s=1,2,…,S runs over all sets of sensor locations and times at which the temperatures are measured. For I sensors each producing L temperature measurements $s = (i-1)L + l$

The first step to retrieve the temperature on the impingement surface, is the parameterization of this function. The equation analogous to (2) reads.

$$T(\mathbf{r},\tau) = \sum_{k=1}^{K} t_k^b N_k(\mathbf{r}) M_n^b(\tau) + \sum_{k=1}^{K} t_k^e N_k(\mathbf{r}) M_n^e(\tau) \tag{7}$$

where the unknown scalars t_k^b and t_k^e are to be determined. Superposition principle produces then a representation

$$T(\mathbf{r},\tau)=\sum_{k=1}^{K}q_k^b\Xi_k^b(\mathbf{r},\tau)+\sum_{k=1}^{K}q_k^e\Xi_k^e(\mathbf{r},\tau)+T_{II}(\mathbf{r},\tau) \tag{8}$$

Where T_{II} is the temperature field corresponding to zero temperature prescribed on $\Gamma_{I,}$, initial condition and boundary conditions on Γ_{II} are taken as in the original problem. Auxiliary fields Ξ_{kb} and Ξ_{ke} satisfy homogeneous boundary conditions on Γ_{II}, homogeneous initial conditions. It is assumed that the temperature on surface Γ_I is equal to $M_n^b(\tau)N_k(\mathbf{r})$ and $M_n^e(\tau)N_k(\mathbf{r})$, respectively. Fields Ξ_{kb} and Ξ_{ke} are readily obtained by invoking a forward solver.

Sampling of (8) produces an overdetermined set of equations of a form

$$\mathbf{T}=\mathbf{J}_t^b\mathbf{t}^b+\mathbf{J}_t^e\mathbf{t}^e+\mathbf{T}_{II} \tag{9}$$

The entries of the sensitivity matrix are defined analogously to (5). The unknown parameters $\mathbf{q}^b$, $\mathbf{q}^e$, $\mathbf{t}^b$ and $\mathbf{t}^b$ are evaluated from the least square fit of the model equations (6) and (9) and the measured temperatures at the same points and times. Denoting by $\hat{T}_s$ s=1,2,…,S subsequent measured temperatures, the least squares problem becomes

$$\min\varphi=\sum_{s=1}^{S}[\hat{T}_s-T_t(\mathbf{r}_i,\tau_l,\mathbf{q}^b,\mathbf{q}^e)]^2+\sum_{s=1}^{S}[\hat{T}_s-T_t(\mathbf{r}_i,\tau_l,\mathbf{t}^b,\mathbf{t}^e)]^2 \tag{10}$$

To enforce the temporal invariance of the HTC, the present study modifies the least squares formulation (10) by introducing the definition of the convective BC (11).

$$h_k=\frac{q_k^b}{T_f-t_k^b}=\frac{q_k^e}{T_f-t_k^e} \tag{11}$$

Elimination of the heat fluxes from eq (10) by resorting to (11) produces

$$\min\varphi=\sum_{s=1}^{S}[\hat{T}_s-T_q(\mathbf{r}_i,\tau_l,\mathbf{t}^b,\mathbf{t}^e,\mathbf{h})]^2+\sum_{s=1}^{S}[\hat{T}_s-T_t(\mathbf{r}_i,\tau_l,\mathbf{t}^b,\mathbf{t}^e)]^2 \tag{12}$$

where T_q is a temperature from the heat flux retrieval and T_t an analogues one from the temperature retrieval procedure. System (12) has been solved using the Levenberg Marquardt technique. Standard formulation of the Levenberg Marquardt algorithm requires calculation of the residuals of the set of equations and recalculating the Jacobian at each step of the iterative procedure. Considering that the generation of the set of equations requires a solution of a forward problem, it is the most time consuming part of the procedure. For the problem at hand however, the entries of the Jacobi matrix are assembled from simple mathematical operations on the sensitivity matrices $\mathbf{J_q}$ and $\mathbf{J_t}$ arising eqs (6) and (9). Moreover, evaluation of the residual of the equations requires only matrix vector multiplication. Therefore the developed algorithm is fast.

5 RESULTS

In this paper the HTC was retrieved by direct and inverse analyses for three different nozzle diameters equal to 5, 6 and 7mm. For each nozzle two distances from the sample equal to 5 and 10 diameters, has been tested. For all cases results of the inverse analysis were compared with the CFD simulations using two measures. The validation of the inverse technique is carried out by comparing:

- distribution of the HTC coefficients predicted by forward CFD simulations and the inverse technique.
- temporal variation of temperature predicted by CFD, measurements and inverse technique

The second comparison requires solution of additional forward problem. As the inverse procedure retrieves only the values of the HTC at the impinged surface, the values of the temperatures at the measured surface cannot be evaluated. Therefore the retrieved spatial distribution of the HTC are prescribed as an input in a simple forward problem in the solid and the resulting temperature field is then compared with the measurements and findings from the CFD simulation.

The results of the inverse analysis depend on the assumed initial temperature field. As mentioned previously, the assumption of the uniform initial temperature field introduces some error. To reduce this influence an excess of temperature over the initial one was retrieved instead the actual temperature. It was done simply by subtracting, from every pixel of the recorded image, the value initially present in the same location. Figure 6 shows comparison of the HTC retrieved with this two ways. Additionally the root mean square temperature errors were compared.

Standard ΔT , K	Excess ΔT , K
0.23	0.21

Table 1: Root mean square temperature difference.

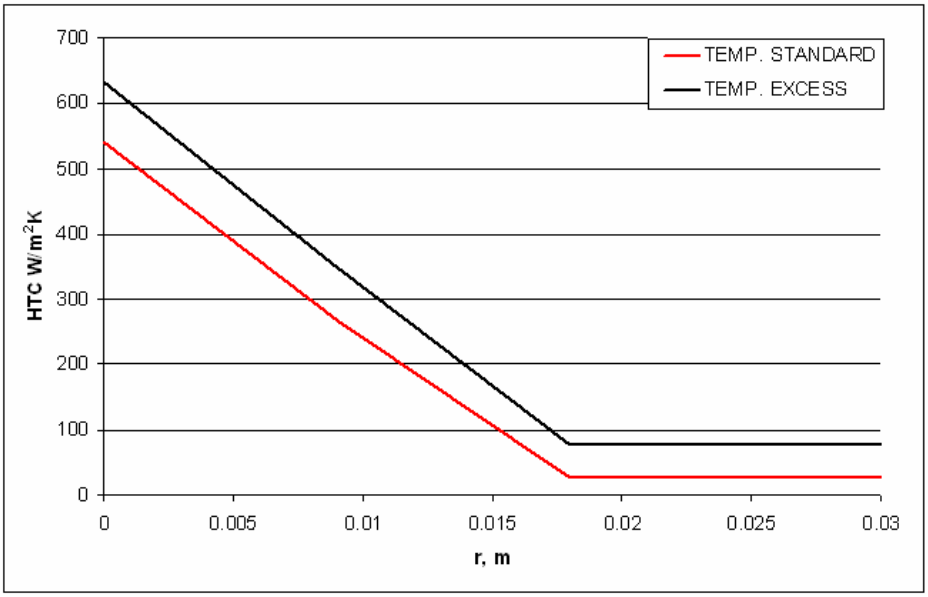

Figure 6: Influence of the initial temperature field on the solution.

Table 1 shows, that if the excess of the temperature is retrieved, the solution is more accurate. The temperature error for the presented case is 10% lower comparing with the case where absolute temperature was retrieved. For all calculated cases the same behavior was observed. The temperature error was between 5 and 23% lower when the excess of the temperature was retrieved.

The spatial distribution of the HTC retrieved by the forward analysis and inverse procedure, versus the distance from the stagnation point, for 5mm nozzle, are presented in

Figure 7. Results of the inverse analysis reveal that the HTC is maximal at the impingement point and that it decreases rapidly with the increase of the radial distance from the impingement point. For the smallest tested nozzle, the CFD analysis shows an existence of two secondary maxima present in the turbulence transition region for the case of five diameters distance between the nozzle and the target. When the nozzle was moved further from the sample the spatial distribution becomes more smooth. For all cases the minimum value of HTC is only 10% of the peak one. The overall value of the HTC, for the stagnation and transition zones, reported by the inverse algorithm is about 30% lower than

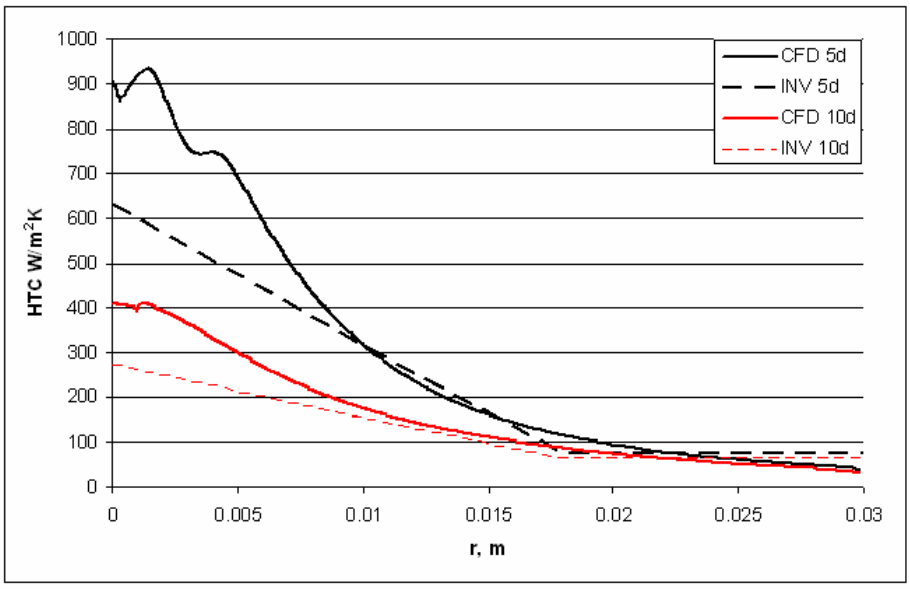

Figure 7: Spatial distribution of the HTC for 5mm nozzle.

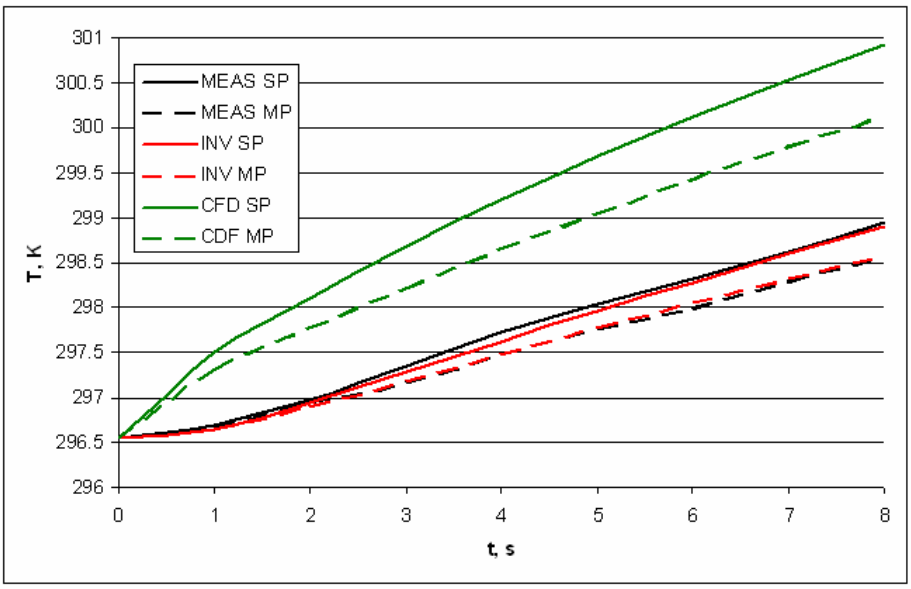

Figure 8: Spatial distribution of the temperature for 5mm nozzle.

the CFD one. The results are the practically the same for distance from the stagnation point grater than 30% of sample radius. The comparison of the temperature is shown in Figure 8. Temperature in two points were compared. SP is the stagnation point, where the centre of the jet hits sample. Second point, MP is located 8mm away from the stagnation point. Both points are located at the outer surface, where the measurements are taken. The comparison shows

that the temperature field obtained for inverse distribution of the HTC is closer to the measured temperatures than the one from the direct simulation. It leads to the conclusion that even the SST k-ω model overpredicts the HTC at the stagnation and transition zones. The biggest temperature differences are present for the first second of the simulation. The over prediction of the temperature may indicate that CFD may not accurately model the initial flow impingement phase.

For larger nozzles the situation is analogous. For 6 and 7mm nozzles and both 5 and 10 diameter distances the HTC obtained from the direct simulation are higher in the

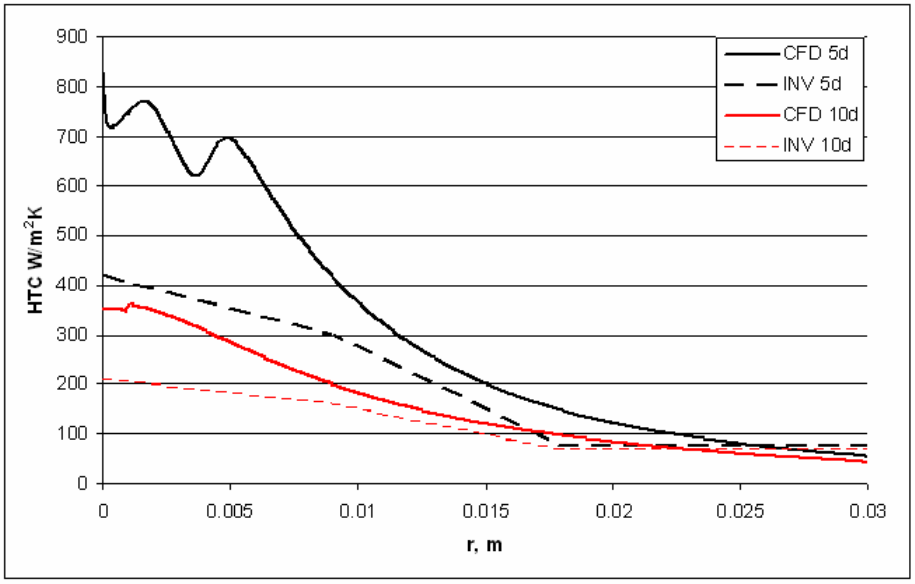

Figure 9: Spatial distribution of the HTC for 6mm nozzle.

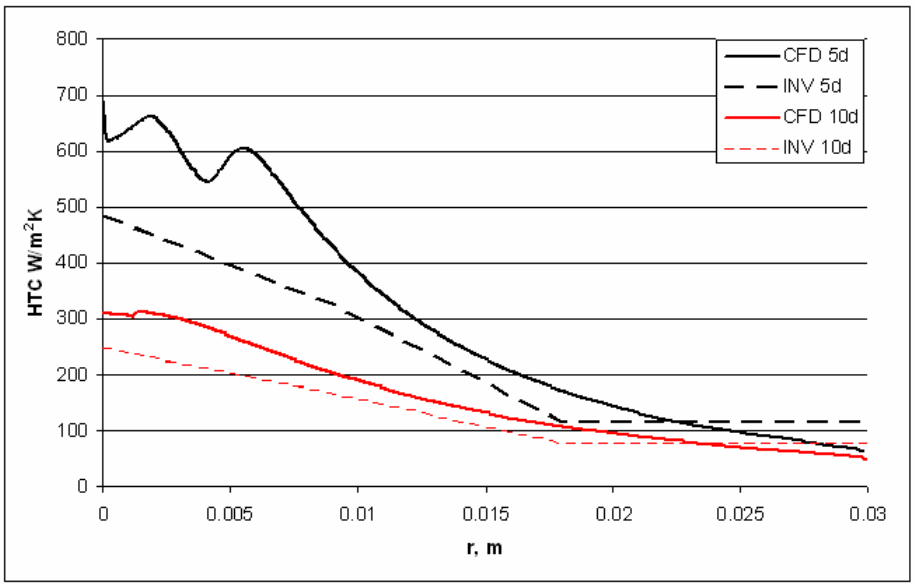

Figure 10: Spatial distribution of the HTC for 7mm nozzle.

stagnation and transition zone. For all cases results of the inverse procedure assume maximum HTC value at stagnation point, while for direct simulation the maximal value is always shifted. The direct analysis reveals existence of additional maxima that are typical to the flow transition zone. Those secondary maxima are more distinct for the nozzle placed closer to the sample as the outer layer of jet strongly affects the flow sliding along the sample.

	Inverse ΔT , K	CFD ΔT , K
5mm 5d	0.38	2.88
5mm 10d	0.21	2.17
6mm 5d	0.27	2.57
6mm 10d	0.19	2.05
7mm 5d	0.36	2.68
7mm 10d	0.23	1.85

Table 2: Root mean square temperature difference for different nozzle configuration.

Comparison of the temperatures shows, that the mean temperature differences are much higher for the direct simulation than for the inverse analysis. It is also important to notice that for smaller nozzle to sample distance the difference for CFD analysis is always higher than for larger distance.

6 CONCLUSIONS

The temperature measurements are closer to the results of the inverse analysis than to that of the CFD simulations. It is important to notice that the inverse analysis does not retrieve the local maximum of the HTC. The attempt to approximated the HTC distribution using more functions placed in the stagnation and transition zone failed to produce feasible results. Such a behavior is a common feature of the inverse procedures. The accuracy of the solution is always a compromise between the stability of the solution and the desired amount of information from the analysis.

The most troublesome problem when in CFD simulations is the usage of proper turbulence model. Even for relatively simple single phase submerged jet the turbulence model plays crucial role in the simulation process. Besides, the computational time for the direct analysis is several orders of magnitude higher than its inverse counterpart. Inverse analysis requires however expensive and time consuming temperature measurements. Additionally it is able to retrieve only low order approximation of the HTC distribution. Therefore, the small number of DOFs in the inverse analysis flattens the HTC value in the stagnation region. As a result, the value of the HTC is under predicted. The temperature comparison shows very good agreement between the inverse results and the measurements. It shows that despite the fact that not all details are retrieved the general agreement is good for all nozzle diameters and nozzle to sample distances. Further development of the code is necessary to improve its stability and make possible to retrieve the HTC using higher number of functions.

REFERENCES

[1] J. Stevens, and B.W. Webb, *Local Heat Transfer Coefficients Under an Axisymmetric, Single-Phase Liquid Jet*, J. Heat Transfer **113**, pp. 71-78 (1991)

[2] B. Sunden, R. Jia and A. Abdon, *Computation of combined turbulent convective and impingement heat transfer*, International Journal of Numerical Methods for Heat & Fluid Flow **14**, pp. 116-133 (2004)

[3] N. Souris, H. Liakos and M. Fonti, *Impinging Jet Cooling on Concave Surfaces*, AIChE Journal **50**, pp. 1672-1683 (2004)

[4] M.A.R. Sharif and A. Banerjee, *Numerical analysis of heat transfer due to confined slot jet impingement on a moving plate*, Applied Thermal Engineering (2008), Available at: doi: 10.1016/j.applthermaleng.2008.03.011

[5] H. M. Hofmann, R. Kaiser, M. Kind and H. Martin, *Calculations of steady and pulsating Impinging jets—an assessment of 13 widely used turbulence models* Num. Heat Transfer, Part B, **51**, pp. 565–583 (2007)

[6] B.A Anderson and R. P. Singh, *Effective heat transfer coefficient measurement during air impingement thawing using an inverse method,* Int. J. Refrigeration **29**, pp. 281-293 (2006)

[7] F. Xu, M.S. Gadala, *Heat transfer behavior in the impingement zone under circular water jet,* Int. J. Heat Mass Transfer **49**, pp. 3785–3799 (2006)

[8] F. Volle, D. Maillet, M. Gradeck, A. Kouachi, M. Lebouché, *Practical application of inverse heat conduction for wall condition estimation on a rotating cylinder*, International Journal of Heat and Mass Transfer **52**, pp.210–221 (2009)

[9] X. Ling, R. G. Keanini and H. P. Cherukuri, *A non-iterative finite element method for inverse heat conduction problems*, Int. J. Numer. Meth. Eng. **56**, pp. 1315–1334 (2003)

[10] A. Ryfa, R.A. Białecki, B. Facchini, L. Tarchi, *Application of the inverse analysis for boundary condition retrieval*, Inv. Probl. in Science Eng. **17** pp 829 - 853, (2009)